

1 **Numerical simulation-based clarification of a fluid-flow system in a seafloor**
2 **hydrothermal vent area in the middle Okinawa Trough**

3
4 **S. A. Tomita¹, K. Koike¹, T. Goto^{1,*}, and K. Suzuki²**

5
6 ¹Department of Urban Management, Graduate School of Engineering, Kyoto University, Kyoto,
7 Japan

8 ²Submarine Resources Research Center, Japan Agency for Marine-Earth Science and
9 Technology (JAMSTEC), Kanagawa, Japan

10 *Now at Graduate School of Life Science, University of Hyogo, Hyogo, Japan

11
12 Corresponding author: S. A. Tomita (tomita.shohei.57n@st.kyoto-u.ac.jp)

13
14 **Key Points:**

- 15 • Numerical simulation of multiphase fluid flow revealed regional temperature, fluid-flow
16 patterns, and physical property distributions.
- 17 • Integration of results with geologic interpretations provided a plausible generation
18 mechanism of seafloor massive sulfide deposits.
- 19 • Formation of caprocks below the seafloor induces boiling and lateral flow of hydrothermal
20 fluid and consequently, the deposit generation.

21 **Abstract**

22 Despite many studies on seafloor hydrothermal systems conducted to date, the generation
23 mechanism of seafloor massive sulfide (SMS) deposits is not yet fully understood. To elucidate
24 this mechanism, this study clarifies the three-dimensional regional temperature distribution and
25 fluid flow of a seafloor hydrothermal system of the Iheya North, middle Okinawa Trough. Lateral
26 flow and boiling of hydrothermal fluids below the seafloor were the main features found by the
27 simulation, leading to an interpretation of two-layered SMS deposit generation as follows.
28 Hydrothermal fluids discharging from black smokers first formed the upper SMS deposits on the
29 seafloor. Caprocks formed below the seafloor, and the above-mentioned occurrences were then
30 induced under the caprocks. In the present system, vapor-rich hydrothermal fluids poor in metals
31 are discharged from the vents as white smokers, whereas liquid-dominated hydrothermal fluids
32 rich in metals flow laterally below the caprocks, forming lower SMS deposits tens of meters below
33 the seafloor.

34

35 **Plain Language Summary**

36 Seafloor hydrothermal activity occurs in a system, called seafloor hydrothermal system, in which
37 the seawater heated by magma circulates under the seafloor, forming seafloor massive sulfide
38 (SMS) deposits. Recently, SMS deposits attract interests as a new metal resource. To develop SMS
39 deposits efficiently, specification of candidate sites by considering their origins is uppermost
40 important. Although many studies on the seafloor hydrothermal systems have been implemented
41 so far, generation mechanism of SMS deposits is not yet fully understood. To understand this
42 mechanism, we applied a hydrothermal flow simulation and clarified the temperature distribution
43 and fluid flow in the Iheya North hydrothermal field, southwestern Japan. The result revealed that
44 lateral flow and boiling of hydrothermal fluids occur below the seafloor, which suggested a
45 generation mechanism as follows. In the old hydrothermal system, hydrothermal fluids rich in
46 metals flowing out from the vents formed SMS deposits on the seafloor. Then, impermeable
47 caprocks formed below the seafloor, resulting in lateral flow and boiling of the hydrothermal fluids
48 under the caprocks. In the present system, vapor-rich hydrothermal fluids poor in metals are flowed
49 out from the vents, while liquid-dominated hydrothermal fluids rich in metals flow laterally below
50 the caprocks, forming SMS deposits below the seafloor.

51

52 **1 Introduction**

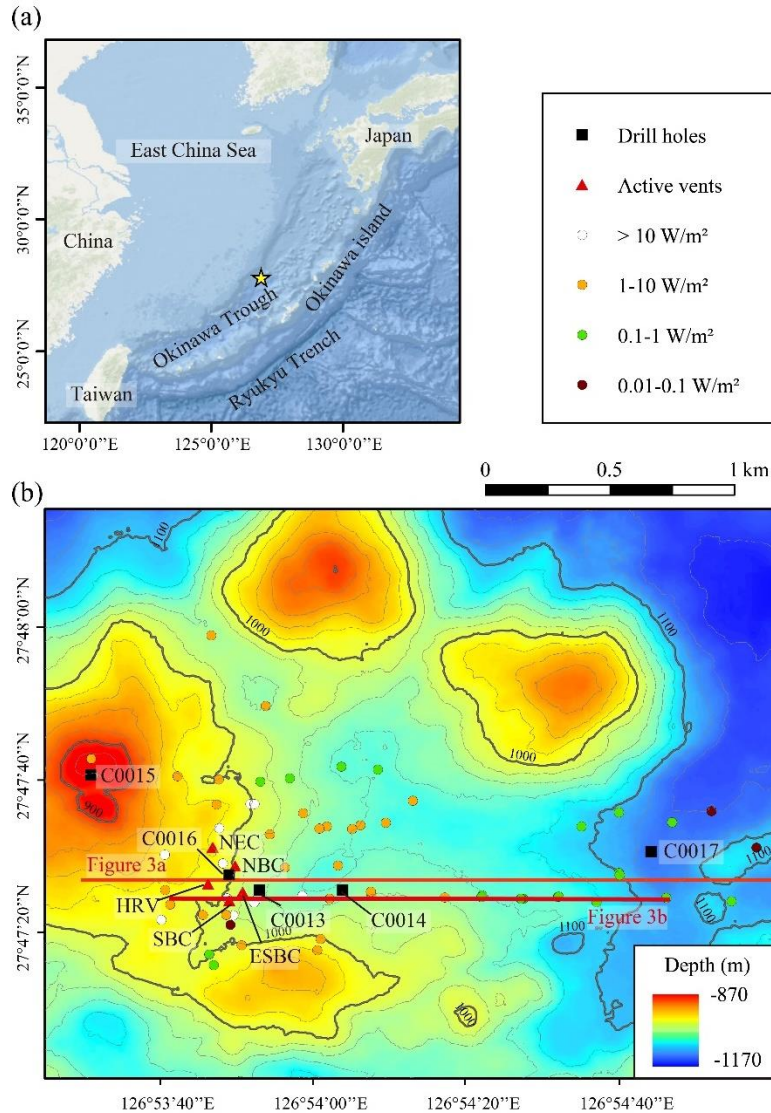
53 Recent rapid expansion of the world economy, population growth, rising demand for and prices of
54 metals, and uneven distribution of resources induce global risks against the stable supply of metal
55 resources (Lusty & Gunn, 2015; Bardi et al., 2016). For the supply, in the exploration of metal
56 deposits, deeper and deeper parts of the crust are being explored, and efforts are extending to the
57 seafloor from the land. In these zones, finding new deposits becomes more and more difficult
58 because of decreases in the amount and spatial resolution of survey data.

59 Because hydrothermal circulation below the seafloor promotes chemical reaction, heat transfer,
60 and mutual interaction between the crust and ocean (Stein & Stein, 1992; Alt, 1995; Tivey, 2007),
61 more than 300 high-temperature vent sites, which are potential fields of metal deposits, have been
62 found to date in mid-ocean ridges (65%), along volcanic arcs (12%), and at back-arc spreading

63 centers (22%) (Hannington et al., 2011). Seafloor massive sulfide (SMS) deposits are the most
64 typical type formed in such hydrothermal systems accompanying high contents of base metals
65 (copper, zinc, and lead) and precious metals (silver and gold) (Spagnoli et al., 2016). SMS deposits
66 are regarded as important near-future mining targets because of their considerable reserves and
67 high metal grades (Lipton, 2012). For efficient mining and development, understanding the
68 locations, configurations, grade distributions, and genesis of such deposits is of the utmost
69 importance.

70 Of particular interest in SMS deposits is the presence of two types, one formed in seafloor mounds
71 and black smoker chimneys under oxic environments and another formed below the seafloor by
72 mineral replacement (Tornos et al., 2015). Co-existence of these types was estimated recently from
73 a two-layered low resistivity zones (of 0.2 Ohm-m or less) by a marine electrical resistivity
74 tomography in the Iheya North Knoll in the mid-Okinawa Trough, southwest of Japan (Ishizu et
75 al., 2019). The structure was interpreted as two mineralization zones on the seafloor and at about
76 40 m below seafloor (mbsf). In addition, similar two or multi-layered SMS deposits were also
77 found by drillings in the Okinawa Trough (Saito et al., 2015; Yoshizumi et al., 2015). To date,
78 various SMS mineralization models have been developed (Tornos et al., 2015). However, most
79 are based on qualitative, geological observations, and the concrete physical setting that caused
80 generation of the deposits (temperature, pressure, heat flux, and fluid flow) has not yet been
81 elucidated; for example, the above-mentioned two-layered mineralization structure has not been
82 explained by any quantitative models. The physical setting can be elucidated only through
83 numerical simulation, because it is not possible to accurately observe the setting and the
84 phenomena that occur there under progress over a long time and a wide area below the seafloor.

85 Based on that background, this study aims to build a three-dimensional (3D) numerical model that
86 can correctly represent a seafloor hydrothermal system in a back-arc basin with geological,
87 hydrological, and thermal constraints, clarify the above physical setting, and present a generation
88 mechanism of the two-layered SMS structure by selecting the Iheya North Knoll as a case area
89 (Figure 1a). Two or more mineralization styles are commonly mixed in SMS deposits (Tornos et
90 al., 2015). Therefore, this study, perhaps the first study conducted for the above purposes, can
91 contribute to understanding the generation setting of complex (two-layered or multilayered) SMS
92 deposits in other areas.



93

94 **Figure 1.** (a) Location of the Iheya North hydrothermal field in the middle Okinawa Trough
 95 marked by a star symbol and (b) bathymetry map of the study area with IODP drilling sites (black
 96 squares), active vent sites (red triangles), and heat flux measurement points (circles as in the legend,
 97 after Masaki et al., 2011). Two red lines show the locations of Figures 3a and b.

98

99 2 Data and Methods

100 The study area is situated in a back-arc basin between the Ryukyu arc-trench system and the
 101 Eurasian continent (Figure 1a); the main hydrothermal area is 500 m × 300 m in size (Figure 1b).
 102 Nine sites of representative active hydrothermal vents have been discovered in this area
 103 (Kawagucci et al., 2011); among them, the North Big Chimney (NBC) is known to have the highest
 104 temperature (311°C) and the largest flow rate recorded thus far (Takai & Nakamura, 2010),
 105 suggesting that the NBC is located on the main flow path.

106 The Iheya North Knoll is composed of i) volcanic rocks forming knolls and ii) thick sediments
107 over the rocks in the central depression; volcanoclastic pumiceous deposits with widely distributed
108 hard layers, perhaps impermeable caprocks, are estimated to be the main sedimentary components
109 based on seismic survey results (Tsuji et al., 2012). Detailed lithology was revealed by drilling
110 surveys at five sites in a program of the Integrated Ocean Drilling Program (IODP) Expedition
111 331 (Figure 1b) (Takai et al., 2011): the sediments are alternating sequences of hard low-porosity
112 and porous pumiceous layers, mainly composed of pelagic and hemipelagic mud and volcanoclastic
113 pumiceous deposits with hydrothermal alteration. Abundant anhydrite greatly reduces the porosity
114 by filling voids in sediments, and consequently forms the low-porosity layers. Anhydrite
115 precipitates from hydrothermal fluid when mixed with seawater (Lowell & Yao, 2002; Lowell et
116 al., 2003). Low-porosity layers rich in anhydrite are regarded to act as impermeable caprocks that
117 blocks vertical fluid flows.

118 Because back-arcs exist under extensional tectonic settings, normal faults, tensile fractures, and
119 fracture zones develop parallel to the extension axis and act as fluid conduits (Sahlström et al.,
120 2018). Following this general rule, several N–S faults are developed in the study area, on which
121 the main hydrothermal mounds are located (Figure 1b). Research on modern (Tivey & Johnson,
122 2002; Arai et al., 2018) and fossil hydrothermal systems (Coogan et al., 2006) has drawn an image
123 wherein hydrothermal upflows are concentrated in tube-like conduits, which presumably continue
124 to the reaction zone (Tivey & Johnson, 2002). In fact, several tube-like conduits under mounds
125 were detected from the seismic survey results in the Okinawa Trough (Arai et al., 2018; Tsuji et
126 al., 2012), including a tube-like seismically transparent structure, which probably represents a
127 conduit, under the NBC mound (Takai et al., 2010).

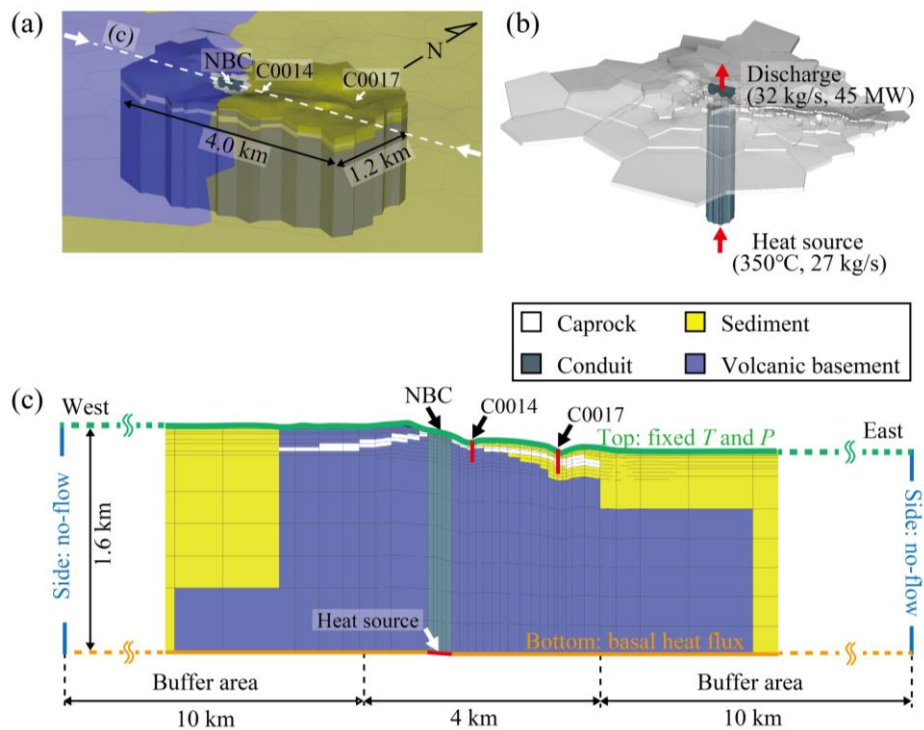
128 Using the above-mentioned accessible geological and geophysical data, a numerical model of the
129 study area, 1.2 km (N–S) \times 4.0 km (E–W) \times 1.6 km (vertical below the seafloor) in size, was
130 constructed (Figure 2) to simulate hydrothermal fluid flow based on Darcy's law and the mass and
131 energy conservation equations. The TOUGH2 software was used for the simulation because of its
132 high capability of analyzing gas–liquid two-phase flow and 3D heat flow (Pruess et al., 1999). A
133 buffer zone 10 km in size was set around the model domain (Figures 2a and c), and the domain
134 was discretized by Voronoi cells with 0.5 m to 500 m thickness from the shallow to deep parts and
135 30 m to 2000 m side length from the middle conduit to domain peripheral zones (Figure 2a). The
136 bathymetric data of the top of the domain were acquired by a multibeam echosounder system
137 (MBES) during several cruises. We set the initial conditions as hydrostatic pressure and 4°C at the
138 seafloor with the average thermal gradient in the study area, 0.12 °C/m, except for the vent sites
139 thermal gradient (Masaki et al., 2011); the surface boundary condition was set as a permeable
140 boundary of the seafloor with constant temperature, 4°C, and hydrostatic pressure, and the side
141 and bottom boundaries were set as impermeable.

142 To clarify the general fluid flow pattern and temperature and pressure distributions, the model
143 domain was simply divided into four geologic elements, conduit, caprock, sediment, and volcanic
144 basement, by excluding geological and hydrological heterogeneities. These elements were
145 assigned in the model domain based on the drilling and seismic survey data. A highly permeable
146 conduit 300 m in diameter was set vertically from the seafloor to the bottom of the model domain
147 as the main discharge area, by locating the NBC as the center of conduit (Figure 2b). Distributions
148 of the volcanic basement, sediment, and a continuous caprock layer 5 m to 100 m in thickness
149 were set following the report of Takai et al. (2011) (Figure 2c). In addition, for the physical rock
150 properties, the density, porosity, and thermal conductivity of the four elements were set based on

151 drilling survey data, and permeability was set based on the literature data described in Text S1 (see
152 also Table S1).

153 The validity of the constructed calculation model was checked by comparing the calculated
154 temperature and heat flux with those obtained by measurement. A wide range of heat flux (0.01–
155 100 W/m²) was observed at 78 points with exceedingly high values around the NBC mound
156 (Masaki et al., 2011). A noteworthy trend was that heat flux decreased with increasing distance
157 from the mound (Figure 1b) to very low heat flux (< 0.1 W/m²) 2 km from the mound, suggesting
158 an occurrence of several-km-scale fluid circulation. In addition, temperature logging data were
159 obtained at Sites C0014 and C0017 (Figure 3d) (Takai et al., 2011). Temperature data obtained at
160 the distal flank at Site C0017 showed 44°C at 112 mbsf and 90°C at 151 mbsf, which imply cold
161 seawater recharge into the hydrothermal system. In contrast, the temperature at Site C0014 at the
162 intermediate flank was 22°C at 6.5 mbsf, and a high thermal gradient was observed below 10 mbsf
163 with temperatures of 55°C at 16 mbsf, 150°C at 47 mbsf, and 210°C at only 50 mbsf. The
164 temperature profiles at Sites C0014 and C0017 did not show simple increases with depth,
165 suggesting the occurrence of lateral flow.

166 The injection rate and discharge rate at the conduit from the bottom and top boundaries,
167 respectively, and the permeabilities of the four elements were adjusted with trial-and-error
168 approaches so that the heat flux and temperature differences would be acceptably small with
169 consideration of heat balance, as explained in Text S2. The resultant injection rate and discharge
170 rate with the best matches were 27 kg/s (= 4×10^{-4} kg/(s·m²)) of 350°C fluid and 32 kg/s (= 45
171 MW heat flow), respectively. Under those conditions, the steady state was simulated.



172

173 **Figure 2.** Calculation model. (a) Perspective view of the model domain with a buffer zone of 10
174 km, shown as semitransparent, set around the domain. Voronoi cell sizes become smaller toward
175 the domain center. The broken white line shows the location of Figure 2c. (b) Distributions of a

176 caprock layer and a vertical conduit zone. (c) Detailed configuration of cells and geologic structure
177 composed of four elements along an E–W cross-section in Figure 2a with the model size and
178 boundary conditions. The cell thickness was set as 0.5 m (thinnest) near the seafloor (the top
179 boundary), because the heat fluxes were measured at the top subsurface below the seafloor (Masaki
180 et al., 2011), and the thickness gradually increases with depth, with 0.5 m for top five layers, 10 m
181 for the next five layers, 25 m for six layers, and 200 m for the bottom seven layers.

182

183 **3 Results and Discussion**

184 The steady state flows are mostly upflows along the conduit and discharge from the seafloor, and
185 partly lateral flows along the caprock form a mushroom-shaped high-temperature region (Figure
186 3a; see also Figure S1 in a cross-section view). Another main flow is descending low-temperature
187 seawater from the seafloor near the volcanic ridge, about 2 km away from the NBC mound at the
188 eastern Site C0017, toward the conduit, which subsequently induces flow circulation. The
189 occurrences of lateral flow below the caprock and downward seawater flow in that place agree
190 with interpretations based on the chemical compositions of the pore waters (Ishibashi et al., 2017)
191 and heat flux and seismic survey data (Masaki et al., 2011; Tsuji et al., 2012).

192 The correctness of the simulation results can be confirmed by the findings that the calculated heat
193 fluxes almost agree with the measured ones (Figure 3b) and that the calculated temperatures
194 generally agree with the measured ones except for the underestimation for the deepest, 50 mbsf
195 data of Site C0014 (Figure 3d). The consistency of heat flux can be more clearly confirmed by a
196 cross-plot of the calculated and measured heat flux values (Figure 3c). The differences between
197 the calculation and measurement results are attributed to the simplified geologic model that did
198 not incorporate local changes in hydraulic parameters.

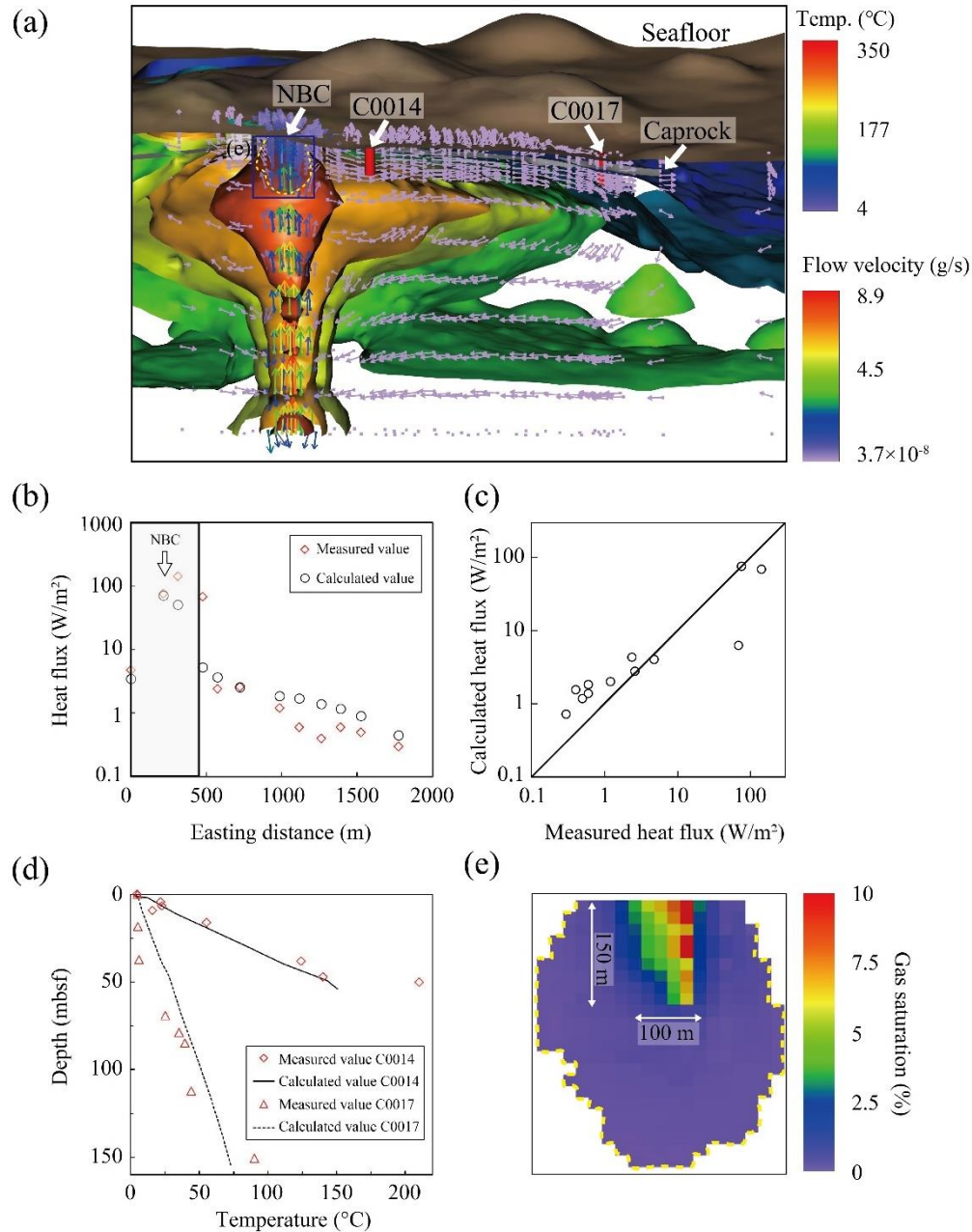
199 A noteworthy feature revealed by the simulation is an occurrence of boiling in the depth range
200 between the surface of the NBC and 150 mbsf in the conduit, caused by a pressure drop at the top
201 of the ascending hydrothermal fluids (Figure 3e). The gas saturation rate reaches a maximum
202 (10%) just below the NBC and decreases gradually toward the surroundings. This occurrence of
203 boiling in the uppermost subseafloor near the NBC can be confirmed by consistency with the
204 observations that all the vents in the study area, including the NBC, emit white fumes (i.e., white
205 smokers) (Chiba et al., 1996) and that many of the vent fluids in this area were Cl-depleted
206 (Kawagucci et al., 2011).

207 To further check the validity of the calculation model, a sensitivity analysis was implemented as
208 described in Text S3 (see also Figures S2 and S3). Models without either the conduit or caprock
209 could not reproduce the measured temperatures and heat fluxes. This mismatch was caused by the
210 nonoccurrence of lateral flows in the shallow subseafloor. Consequently, the importance of the
211 conduit and caprock for hydrothermal fluid flow and their correct setting in this study are
212 demonstrated.

213 Distributions of massive and granular sulfide minerals were observed near the NBC seafloor (Site
214 C0016) and near the shallow subseafloor of Sites C0013 and C0014 (Yeats et al., 2017), and the
215 formation of two-layered SMS deposits was estimated by Ishizu et al. (2019), as mentioned above.
216 This two-layered structure can be considered to have been caused by the boiling of hydrothermal
217 fluids and lateral flows in the shallow subseafloor. Both the simulation result and field observations
218 suggested the occurrence of two-phase separation into vapor- and liquid-rich fluids in the

219 uppermost subseafloor near the NBC. Through this phase separation, metal components in the
220 fluids become concentrated in the liquid phase, and sulfide minerals precipitate (Kawagucci et al.,
221 2013) by the fractionation of chemical species, the pH of the fluids increases, and metal solubility
222 decreases (Drummond & Ohmoto, 1985). The vapor-rich, light fluids poor in metal components
223 ascend and are probably discharged from the vents, which is concordant with the fact that all the
224 vents in the study area are white smokers, as mentioned above, in which sulfide minerals are
225 scarcely contained. Therefore, sulfide minerals on the seafloor probably precipitated from past
226 black smokers. At the same time, the liquid-rich fluids are trapped below the caprock, as confirmed
227 through a drilling survey (Kawagucci et al., 2013), and their lateral flows must have caused sulfide
228 mineral precipitation.

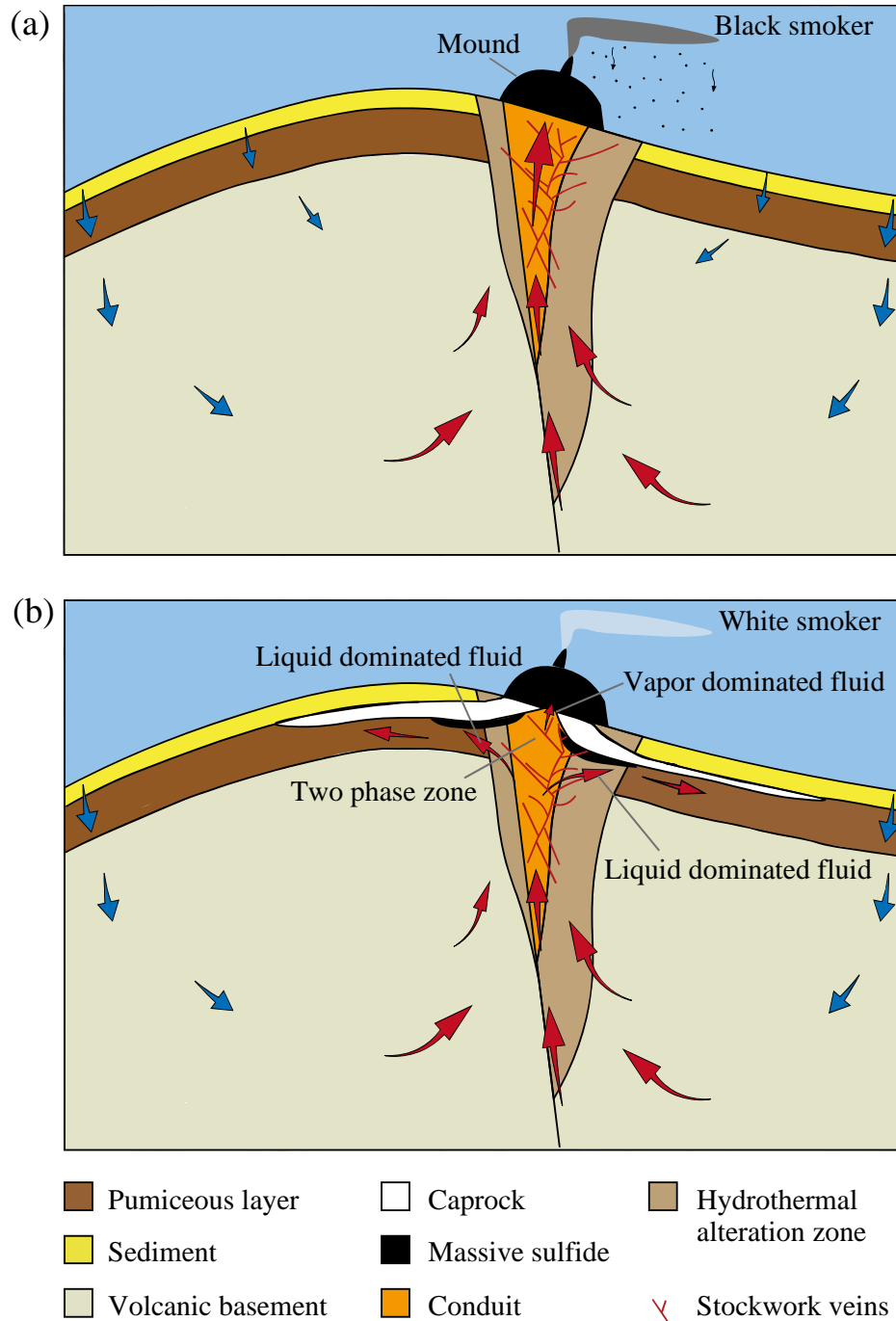
229 Based on the above considerations, we propose a two-stage generation scenario of the two-layered
230 SMS deposit in the Iheya North Knoll as follows. In the early stage, high-temperature
231 hydrothermal fluids ascended along the conduit and discharged from the vents as black smokers
232 without boiling below the seafloor, and considerable amounts of sulfide minerals then precipitated
233 on the seafloor from the black smokers by mixing with the seawater (Figure 4a). Long-term
234 precipitation formed a mound, and that mound acted to seal the hydrothermal fluid flows in the
235 later stage; consequently, the fluid flows became concentrated in the vent (Tivey, 2007; Fouquet,
236 1997). The sealing was intensified by the distribution of low-permeability hemipelagic sediments
237 in the shallow subseafloor around the mound. Through mixing of the hydrothermal fluids with the
238 seawater in the mound, anhydrite precipitated and filled the rock voids under fluid temperatures
239 of 200°C or more (Fouquet, 1997; Ishibashi et al., 2017). In addition, the rocks were
240 hydrothermally altered and changed partly to clay minerals with decreasing permeability
241 (Takahashi, 1995). These rocks containing anhydrite and clay minerals in voids became
242 impermeable caprock, which blocked mixing of the hydrothermal fluids and seawater; in addition,
243 the conduit top gradually became less permeable, resulting in flow being diverted horizontally
244 (Koski et al., 1994; Tivey et al., 1995) into the highly permeable volcaniclastic layer (Figure 4b).
245 Because of the effect of the caprock to suppress mixing, the fluid temperature increased, and
246 consequently, boiling occurred at the conduit top, and vapor-rich fluids were discharged from the
247 vents as white smokers, as is occurring at present. At the same time, the liquid-rich fluids rich in
248 metal components flowed laterally under the caprock and precipitated sulfide minerals, mainly by
249 boiling and/or by conductive cooling.



250

251 **Figure 3.** Simulation results and verification. (a) 3D view of iso-temperature surfaces and fluid
 252 flow vectors (arrows) on an E–W cross-section along the profile shown in Figure 1b. Boiling zone
 253 around the NBC is delineated by the broken yellow line. The thick red lines, brown surface, and
 254 gray surface in the shallow subseafloor denote the seafloor drillings with site names, the seafloor,
 255 and the caprock layer, respectively. (b) Comparison of calculated heat fluxes with the measurement
 256 data after Masaki et al. (2011). The easting distance is along the profile shown in Figure 1b. The
 257 gray hatched part from 0 to 450 m distance denotes the active hydrothermal area. (c) Cross-plot of
 258 calculated heat flux and measured ones. (d) Comparison of calculated temperatures with the
 259 measurement data at Sites C0014 and C0017 after Takai et al. (2011). (e) Vertical cross-section of
 260 gas saturation distribution in the boiling zone shown in Figure 3a.

261



262

263 **Figure 4.** Conceptual model of the two-stage mineralization process. (a) Early-stage
 264 mineralization model in which black smokers discharging from the seafloor were cooled by the
 265 seawater and sulfide minerals precipitated from the vents, forming SMS deposits on the seafloor.
 266 Long-term precipitation formed a mound around the vent. (b) Late-stage mineralization model in
 267 which impermeable portions composed of anhydrite and the clay minerals-bearing mound, and
 268 sediment induce lateral flows and boiling of fluids in the conduit top. Gas-phase dominated fluids
 269 are discharged from the vent as a white smoker. In contrast, liquid-phase dominated fluids rich in
 270 metal components flow laterally below the caprock and form the lower ore body because of boiling

271 and/or conductive cooling. The blue and red arrows denote fluid flows of relatively low- and high-
272 temperature seawaters, respectively.
273

274 **4 Conclusions**

275 In this study, a simple, but essential subseafloor geologic model was constructed to clarify the
276 regional temperature, fluid-flow patterns, and physical property distributions in a hydrothermal
277 system of a back-arc basin, by selecting the Iheya North Knoll, middle Okinawa Trough, southwest
278 Japan as an example. This clarification was achieved by a numerical simulation of multi-phase
279 fluid using TOUGH2 with geological, hydrological, and thermal constraints. The most important
280 finding of this study is that the fluid flow is essentially controlled by the presences of a caprock
281 layer and conduit. The resultant flow features were that the hydrothermal fluids ascend along the
282 conduit toward the seafloor and a portion of them flow laterally below the caprock, as observed
283 by a drilling survey. Because of the presences of the caprock and conduit, the calculated
284 temperatures and heat fluxes were consistent with the measured ones, and the boiling location was
285 in accord with the observed one.

286 In the study area, development of the two-layered SMS deposit in the study area was interpreted
287 using electrical resistivity tomography. Based on the simulation results and the preceding
288 measurements and observations, a generation mechanism of this two-layered SMS deposit was
289 proposed as formation by two stages of mineralization. In the early stage, hydrothermal fluids were
290 discharged as black smokers rich in metals, and by mixing with the seawater, sulfide minerals from
291 the smokers were deposited on the seafloor. In the later stage, the conduit gradually became less
292 permeable over time, which induced lateral flows in a highly permeable volcanoclastic layer, and
293 consequently, caprock was generated by the precipitation of anhydrite and clay minerals in the
294 layer. Because of the caprock, the temperature of the hydrothermal fluids increased and boiling
295 occurred. The vapor-rich fluids were discharged as white smokers from the vents, whereas the
296 liquid-rich fluids, flowing laterally below the caprock, formed the lower SMS deposits mainly by
297 boiling.
298

299 **Acknowledgments, Samples, and Data**

300 Data is available through Takai et al. (2011) and Masaki et al. (2011). This work was supported
301 by the Council for Science, Technology and Innovation (CSTI), Cross-ministerial Strategic
302 Innovation Promotion Program (SIP), “Next-generation technology for ocean resources
303 exploration” (Funding agency: Japan Agency for Marine-Earth Science and Technology,
304 JAMSTEC).

305 **References**

- 306 Alt, J. C. (1995). Seafloor Processes in Mid-Ocean Ridge Hydrothermal Systems. *Seafloor*
307 *Hydrothermal Systems: Physical, Chemical, Biological, and Geological Interactions*, 91,
308 85-114. <https://doi.org/10.1029/GM091p0085>
- 309 Arai, R., Kodaira, S., Takahashi, T., Miura, S., & Kaneda, Y. (2018). Seismic evidence for arc
310 segmentation, active magmatic intrusions and syn-rift fault system in the northern Ryukyu
311 volcanic arc. *Earth, Planets and Space*, 70(1). <https://doi.org/10.1186/s40623-018-0830-8>
- 312 Bardi, U., Jakobi, R., & Hettiarachchi, H. (2016). Mineral Resource Depletion: A Coming Age of
313 Stockpiling?. *BioPhysical Economics and Resource Quality*, 1(4).
314 <https://doi.org/10.1007/s41247-016-0004-x>
- 315 Bear, J. (1972). *Dynamics of Fluids in Porous Media*. New York: American Elsevier.
- 316 Chiba, H., Ishibashi, J., Ueno, H., Oomori, T., Uchiyama, N., Takeda, T., et al. (1996). Seafloor
317 hydrothermal systems at North Knoll, Iheya Ridge, Okinawa Trough. *JAMSTEC Journal*
318 *of Deep Sea Research*, 12, 211-219.
- 319 Converse, D., Holland, H., & Edmond, J. (1984). Flow rates in the axial hot springs of the East
320 Pacific Rise (21 N): Implications for the heat budget and the formation of massive sulfide
321 deposits. *Earth and Planetary Science Letters*, 69(1), 159-175.
322 [https://doi.org/10.1016/0012-821X\(84\)90080-3](https://doi.org/10.1016/0012-821X(84)90080-3)
- 323 Coogan, L., Howard, K., Gillis, K., Bickle, M., Chapman, H., Boyce, A., et al. (2006). Chemical
324 and thermal constraints on focussed fluid flow in the lower oceanic crust. *American*
325 *Journal of Science*, 306(6), 389-427. <https://doi.org/10.2475/06.2006.01>
- 326 Coumou, D., Driesner, T., & Heinrich, C. A. (2008). The structure and dynamics of mid-ocean
327 ridge hydrothermal systems. *Science*, 321(5897), 1825-1828.
328 <https://doi.org/10.1126/science.1159582>
- 329 Drummond, S., & Ohmoto, H. (1985). Chemical evolution and mineral deposition in boiling
330 hydrothermal systems. *Economic Geology*, 80(1), 126-147.
331 <https://doi.org/10.2113/gsecongeo.80.1.126>
- 332 Elderfield, H., & Schultz, A. (1996). Mid-ocean ridge hydrothermal fluxes and the chemical
333 composition of the ocean. *Annual Review of Earth and Planetary Sciences*, 24(1), 191-224.
334 <https://doi.org/10.1146/annurev.earth.24.1.191>
- 335 Fehn, U., & Cathles, L. M. (1979). Hydrothermal convection at slow-spreading mid-ocean ridges.
336 *Tectonophysics*, 55(1-2), 239-260. [https://doi.org/10.1016/0040-1951\(79\)90343-3](https://doi.org/10.1016/0040-1951(79)90343-3)
- 337 Fisher, A., Becker, K., & Narasimhan, T. (1994). Off-axis hydrothermal circulation: Parametric
338 tests of a refined model of processes at Deep Sea Drilling Project/Ocean Drilling Program
339 site 504. *Journal of Geophysical Research: Solid Earth*, 99(B2), 3097-3121.
340 <https://doi.org/10.1029/93JB02741>
- 341 Fouquet, Y. (1997). Where are the large hydrothermal sulphide deposits in the oceans?.
342 *Philosophical Transactions of the Royal Society A: Mathematical, Physical and*
343 *Engineering Sciences*, 355(1723), 427-441. <https://doi.org/10.1098/rsta.1997.0015>
- 344 Freeze, R. A., & Cherry, J. A. (1979). *Groundwater*. Englewood Cliffs, NJ: Prentice Hall.

- 345 Gruen, G., Weis, P., Driesner, T., Heinrich, C. A., & de Ronde, C. E. J. (2014). Hydrodynamic
346 modeling of magmatic–hydrothermal activity at submarine arc volcanoes, with
347 implications for ore formation. *Earth and Planetary Science Letters*, 404, 307-318.
348 <https://doi.org/10.1016/j.epsl.2014.07.041>
- 349 Hannington, M., Jamieson, J., Monecke, T., Petersen, S., & Beaulieu, S. (2011). The abundance
350 of seafloor massive sulfide deposits. *Geology*, 39(12), 1155-1158.
351 <https://doi.org/10.1130/G32468.1>
- 352 Ishibashi, J., Yanagikawa, K., & Takai, K. (2017). A new model for a hydrothermal circulation
353 system and limit of the life (in Japanese with English abstract). *The Journal of the*
354 *Geological Society of Japan*, 123(4), 237-250. <https://doi.org/10.5575/geosoc.2017.0014>
- 355 Ishizu, K., Goto, T., Ohta, Y., Kasaya, T., Iwamoto, H., Vachiratiengchai, C., et al. (2019). Internal
356 structure of a seafloor massive sulfide deposit by electrical resistivity tomography,
357 Okinawa Trough. *Geophysical Research Letters*, 46, 11025-11034.
358 <https://doi.org/10.1029/2019GL083749>
- 359 Kawagucci, S., Chiba, H., Ishibashi, J., Yamanaka, T., Toki, T., Muramatsu, Y., et al. (2011).
360 Hydrothermal fluid geochemistry at the Iheya North field in the mid-Okinawa Trough:
361 Implication for origin of methane in subseafloor fluid circulation systems. *Geochemical*
362 *Journal*, 45(2), 109-124. <https://doi.org/10.2343/geochemj.1.0105>
- 363 Kawagucci, S., Miyazaki, J., Nakajima, R., Nozaki, T., Takaya, Y., Kato, Y., et al. (2013). Post-
364 drilling changes in fluid discharge pattern, mineral deposition, and fluid chemistry in the
365 Iheya North hydrothermal field, Okinawa Trough. *Geochemistry, Geophysics, Geosystems*,
366 14(11), 4774-4790. <https://doi.org/10.1002/2013GC004895>
- 367 Koski, R. A., Jonasson, I. R., Kadko, D. C., Smith, V. K., & Wong, F. L. (1994). Compositions,
368 growth mechanisms, and temporal relations of hydrothermal sulfide-sulfate-silica
369 chimneys at the northern Cleft segment, Juan de Fuca Ridge. *Journal of Geophysical*
370 *Research: Solid Earth*, 99(B3), 4813-4832. <https://doi.org/10.1029/93JB02871>
- 371 LaFlamme, B., Delaney, J., McDuff, R., Miller, V., Robigou, V., Schultz, A., et al. (1989).
372 Observations and experimental studies in the Endeavour hydrothermal field-Summer 1988.
373 *EOS, Transactions, American Geophysical Union*, 70, 1160-1161.
- 374 Lipton, I. (2012). *Mineral Resource Estimate Solwara Project, Bismarck Sea PNG* (Technical
375 Report NI43-101). Retrieved from
376 [http://www.nautilusminerals.com/irm/content/pdf/SL01-NSG-DEV-RPT-7020-](http://www.nautilusminerals.com/irm/content/pdf/SL01-NSG-DEV-RPT-7020-001_Rev_1_Golder_Resource_Report.pdf)
377 [001_Rev_1_Golder_Resource_Report.pdf](http://www.nautilusminerals.com/irm/content/pdf/SL01-NSG-DEV-RPT-7020-001_Rev_1_Golder_Resource_Report.pdf)
- 378 Lowell, R. P., & Yao, Y. (2002). Anhydrite precipitation and the extent of hydrothermal recharge
379 zones at ocean ridge crests. *Journal of Geophysical Research: Solid Earth*, 107(B9), EPM
380 2-1-EPM 2-9. <https://doi.org/10.1029/2001JB001289>
- 381 Lowell, R. P., Yao, Y., & Germanovich, L. N. (2003). Anhydrite precipitation and the relationship
382 between focused and diffuse flow in seafloor hydrothermal systems. *Journal of*
383 *Geophysical Research: Solid Earth*, 108(B9), EPM 3-1-EPM 3-8.
384 <https://doi.org/10.1029/2002JB002371>

- 385 Lusty, P., & Gunn, A. (2015). Challenges to global mineral resource security and options for future
386 supply. *Geological Society, London, Special Publications*, 393(1), 265-276.
387 <https://doi.org/10.1144/SP393.13>
- 388 Magri, F., Akar, T., Gemici, U., & Pekdeger, A. (2010). Deep geothermal groundwater flow in the
389 Seferihisar–Balçova area, Turkey: results from transient numerical simulations of coupled
390 fluid flow and heat transport processes. *Geofluids*, 10(3), 388-405.
391 <https://doi.org/10.1111/j.1468-8123.2009.00267.x>
- 392 Masaki, Y., Kinoshita, M., Inagaki, F., Nakagawa, S., & Takai, K. (2011). Possible kilometer-
393 scale hydrothermal circulation within the Iheya-North field, mid-Okinawa Trough, as
394 inferred from heat flow data. *JAMSTEC Report of Research and Development*, 12, 1-12.
395 <https://doi.org/10.5918/jamstecr.12.1>
- 396 Pruess, K., Oldenburg, C. M., & Moridis, G. (1999). *TOUGH2 user's guide version 2* (Rep. LBNL-
397 43134). Berkeley, CA: Lawrence Berkeley National Laboratory.
398 <https://doi.org/10.2172/751729>
- 399 Raharjo, I. B., Allis, R. G., & Chapman, D. S. (2016). Volcano-hosted vapor-dominated
400 geothermal systems in permeability space. *Geothermics*, 62, 22-32.
401 <https://doi.org/10.1016/j.geothermics.2016.02.005>
- 402 Rona, P. A., & Trivett, D. A. (1992). Discrete and diffuse heat transfer at ASHES vent field, Axial
403 Volcano, Juan de Fuca Ridge. *Earth and Planetary Science Letters*, 109(1-2), 57-71.
404 [https://doi.org/10.1016/0012-821X\(92\)90074-6](https://doi.org/10.1016/0012-821X(92)90074-6)
- 405 Sahlström, F., Dirks, P., Chang, Z., Arribas, A., Corral, I., Obiri-Yeboah, M., & Hall, C. (2018).
406 The Paleozoic Mount Carlton Deposit, Bowen Basin, Northeast Australia: Shallow High-
407 Sulfidation Epithermal Au-Ag-Cu Mineralization Formed During Rifting. *Economic*
408 *Geology*, 113(8), 1733-1767. <https://doi.org/10.5382/econgeo.2018.4611>
- 409 Saito, S., Sanada, Y., Moe, K., Kido, Y. N., Hamada, Y., Kumagai, H., et al. (2015). Identification
410 and characterization of the active hydrothermal deposits in Okinawa Trough, SW Japan:
411 estimates from logging-while-drilling. *AGU Fall Meeting Abstracts*. San Francisco.
412 Retrieved from <https://agu.confex.com/agu/fm15/webprogram/Paper77585.html>
- 413 Schultz, A., Delaney, J., & McDuff, R. (1992). On the partitioning of heat flux between diffuse
414 and point source seafloor venting. *Journal of Geophysical Research: Solid Earth*, 97(B9),
415 12299-12314. <https://doi.org/10.1029/92JB00889>
- 416 Schultz, A., & Elderfield, H. (1999). Controls on the physics and chemistry of seafloor
417 hydrothermal circulation. In J. R. Cann, H. Elderfield, & A. Laughton (Eds.), *Mid-Ocean*
418 *Ridges, Dynamics of Processes Associated with Creation of New Oceanic Crust* (pp. 171-
419 210). Cambridge, UK: Cambridge university press.
- 420 Spagnoli, G., Hannington, M., Bairlein, K., Hördt, A., Jegen, M., Petersen, S., & Laurila, T. (2016).
421 Electrical properties of seafloor massive sulfides. *Geo-Marine Letters*, 36(3), 235-245.
422 <https://doi.org/10.1007/s00367-016-0439-5>
- 423 Stein, C. A., & Stein, S. (1992). A model for the global variation in oceanic depth and heat flow
424 with lithospheric age. *Nature*, 359(6391), 123-129. <https://doi.org/10.1038/359123a0>

- 425 Takahashi, H. (1995). Alteration cap rock formation model —A case study Hosokura ore deposits
426 in northeastern Japan— (in Japanese with English abstract). *Journal of the Geothermal*
427 *Research Society of Japan*, 17(4), 271-284. <https://doi.org/10.11367/grsj1979.17.271>
- 428 Takai, K., Mottl, M., Nielsen, S., & the Expedition 331 Scientists (2010). *Deep hot biosphere*
429 (Integrated Ocean Drilling Program Preliminary Report, 331). Tokyo: Integrated Ocean
430 Drilling Program Management International, Inc. <https://doi.org/10.2204/iodp.pr.331.2010>
- 431 Takai, K., Mottl, M., Nielsen, S., & the Expedition 331 Scientists (2011). *Proceedings of the*
432 *Integrated Ocean Drilling Program* (Vol. 331). Tokyo: Integrated Ocean Drilling Program
433 Management International, Inc. <https://doi.org/10.2204/iodp.proc.331.2011>
- 434 Takai, K. & Nakamura, K. (2010). Compositional, physiological and metabolic variability in
435 microbial communities associated with geochemically diverse, deep-sea hydrothermal vent
436 fluids. In L. L. Barton, M. Mandl, & A. Loy (Eds.), *Geomicrobiology: Molecular and*
437 *Environmental Perspective* (pp. 251-283). Dordrecht: Springer.
438 https://doi.org/10.1007/978-90-481-9204-5_12
- 439 Tivey, M. K. (2007). Generation of seafloor hydrothermal vent fluids and associated mineral
440 deposits. *Oceanography*, 20(1), 50-65. <https://doi.org/10.5670/oceanog.2007.80>
- 441 Tivey, M. K., Humphris, S. E., Thompson, G., Hannington, M. D., & Rona, P. A. (1995). Deducing
442 patterns of fluid flow and mixing within the TAG active hydrothermal mound using
443 mineralogical and geochemical data. *Journal of Geophysical Research: Solid Earth*,
444 100(B7), 12527-12555. <https://doi.org/10.1029/95JB00610>
- 445 Tivey, M. A., & Johnson, H. P. (2002). Crustal magnetization reveals subsurface structure of Juan
446 de Fuca Ridge hydrothermal vent fields. *Geology*, 30(11), 979-982.
447 [https://doi.org/10.1130/0091-7613\(2002\)030<0979:CMRSSO>2.0.CO;2](https://doi.org/10.1130/0091-7613(2002)030<0979:CMRSSO>2.0.CO;2)
- 448 Tornos, F., Peter, J. M., Allen, R., & Conde, C. (2015). Controls on the siting and style of
449 volcanogenic massive sulphide deposits. *Ore Geology Reviews*, 68, 142-163.
450 <https://doi.org/10.1016/j.oregeorev.2015.01.003>
- 451 Tsuji, T., Takai, K., Oiwane, H., Nakamura, Y., Masaki, Y., Kumagai, H., et al. (2012).
452 Hydrothermal fluid flow system around the Iheya North Knoll in the mid-Okinawa trough
453 based on seismic reflection data. *Journal of Volcanology and Geothermal Research*, 213-
454 214, 41-50. <https://doi.org/10.1016/j.jvolgeores.2011.11.007>
- 455 Yang, J., Edwards, R., Molson, J. W., & Sudicky, E. (1996). Three-dimensional numerical
456 simulation of the hydrothermal system within TAG-Like sulfide mounds. *Geophysical*
457 *Research Letters*, 23(23), 3475-3478. <https://doi.org/10.1029/96GL03081>
- 458 Yeats, C. J., Hollis, S. P., Halfpenny, A., Corona, J., LaFlamme, C., Southam, G., et al. (2017).
459 Actively forming Kuroko-type volcanic-hosted massive sulfide (VHMS) mineralization at
460 Iheya North, Okinawa Trough, Japan. *Ore Geology Reviews*, 84, 20-41.
461 <https://doi.org/10.1016/j.oregeorev.2016.12.014>
- 462 Yoshizumi, R., Miyoshi, Y., & Ishibashi, J. (2015). The Characteristics of the Seafloor Massive
463 Sulfide Deposits at the Hakurei Site in the Izena Hole, the Middle Okinawa Trough. In J.
464 Ishibashi, K. Okino, & M. Sunamura (Eds.), *Subseafloor Biosphere Linked to*
465 *Hydrothermal Systems* (pp. 561-565). Tokyo: Springer. https://doi.org/10.1007/978-4-431-54865-2_43
466